

# Vehicle State Estimation and Friction Grids

Ahmad Amine [aminea@seas.upenn.edu], Adithyakrishna Venkatesh Hanasoge [adikvh@seas.upenn.edu],  
Joshua Ernest Pedi Reddy [josherne@seas.upenn.edu]

**Abstract**—In recent years, there has been a surge in autonomous vehicle development. However, even when algorithms perform wonderfully in simulations, transferring this success to the real world is rarely an easy process. As such, bridging the sim-2-real gap is a crucial step in ensuring the safety of autonomous vehicles. In this project, we attempt to decrease the size of this gap by incorporating friction estimates of the terrain that vehicles drive on. The goal is to build a two-stage estimator that first estimates the state of our vehicle (angular and linear speeds) and use these estimates to estimate road friction. Using this estimate of the road friction coefficient  $\mu$ , we can then fuse this information into an occupancy grid, localized using a particle filter to localize estimates of the road friction coefficient at different locations in our map. This algorithm is then tested on the F1/10th autonomous racing platform to obtain the empirical performance metrics of our estimator.

## I. BACKGROUND

Direction control and stability performance of a road vehicle directly relate to forces developed at the tire-road interface, which are mostly limited by the available tire-road coefficient (TRFC). Since unmanned vehicles should be able to perform on a variety of surface conditions, weather conditions and tire conditions and more, the real time knowledge of varying friction is vital for motion control and safe driving of the autonomous vehicles. In our case, friction estimation for an F1/10<sup>th</sup> car was critical as our car would slide and drift due to varying friction conditions and inaccurate estimation of friction available at the tire-road interface.

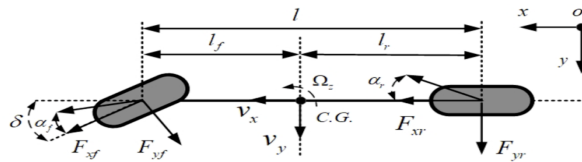


Figure 1: Vehicle Dynamics Model - Single Track

Motivated by practicality, we assume our F1/10<sup>th</sup> car as a single-track bicycle model and also assume roll and pitch are negligible. We also assume zero aerodynamic drag due to the low speeds of our F1/10<sup>th</sup> car. The maximum speed that we drove at was around 6 m/s ( $\approx 21 \text{ km/hr}$ ), and therefore zero aerodynamic drag. The car telemetry that we had access to includes IMU data (lateral acceleration, longitudinal acceleration, yaw

rate, roll, pitch), steering angle from the onboard servo motor, commanded speed, and motor RPM. The motor RPM was only available for dataset 5. We also had access to the specification sheet of the F1/10th car for various parameters of the car.<sup>[1][2]</sup> Notations mentioned in Appendix (Section VII).

## II. RELATED WORK

There exists an extensive literature on estimating vehicle states and road friction estimation. [3] provides an extensive study on tire modeling and concludes with a road-friction estimator which utilizes a least-squares optimizer to estimate the road's friction using a Gauss-Newton algorithm. [4] implements a two-stage Unscented Kalman Filter to decouple vehicle dynamics parameters from vehicle dynamic estimates. [5] demonstrates the use of a Dual Extended Kalman Filter estimator to obtain vehicle states and road friction coefficients. [6] provides a survey of vehicle dynamic state estimation techniques as of March 2018. These techniques also include tire/road friction coefficient estimation. [7] implements a three-stage kalman filter approach that combines the velocity estimates from an EKF as well as the forces estimates from a UKF to estimate the friction coefficients from the third UKF.

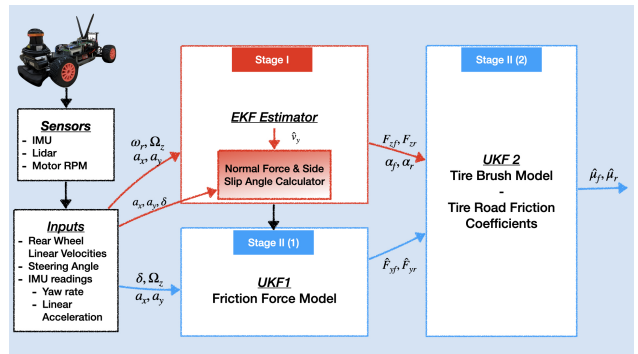


Figure 2: Filtering General Hierarchy

## III. APPROACH

In this project, we will be implementing the approach implemented by [7] but applied to an all-wheel drive car in our case. Additionally, our mean velocity of the rear wheels at the ground interface, can not be obtained from angular speed of the wheels as we do not have

measurements of these speeds. Instead, we estimate this velocity based on our motor's RPM.

#### A. EKF – Estimation of Vehicle Velocity

The first stage in the two stage Tire Road Friction Coefficient (TRFC) estimation estimates vehicle lateral velocity using an Extended Kalman Filter (EKF). The tire side-slip angles are directly related to instantaneous longitudinal and lateral velocities of the vehicle as shown by 1.

$$\begin{aligned}\alpha_f &= \frac{v_y + l_f \omega_z}{v_x} - \delta \\ \alpha_r &= \frac{v_y + l_r \omega_z}{v_x}\end{aligned}\quad (1)$$

We assume small yaw angles and therefore the kinematic relationships between the accelerations and derivatives of the vehicle velocities can be expressed as 2.

$$\begin{aligned}a_x &= \dot{v}_x - v_y \Omega_z \\ a_y &= \dot{v}_y - v_x \Omega_z\end{aligned}\quad (2)$$

Using these relations, we derive the state-space system in the discrete time as equation 3.

$$\begin{aligned}x_k^E &= f^E(x_{k-1}^E, u_k^E) + w_k^E, \text{ where } w_k^E \sim N(0, R^E) \\ z_k^E &= h^E(x_k^E) + v_k^E, \text{ where } v_k^E \sim N(0, Q^E) \\ Q^E &= 10^{-3} \\ R^E &= \text{diag}([10, 10])\end{aligned}\quad (3)$$

The system state  $x_x^E$  and measurement vectors  $z_k^E$  and input vector  $U_e$  are 4 respectively.

$$\begin{aligned}x_k^E &= [v_{x,k}, v_{y,k}]^T \\ z_k^E &= v_{x,k}^m \\ u_k^E &= [a_{x,k}, a_{y,k}, \Omega_z]^T\end{aligned}\quad (4)$$

Since we assume a single track system,  $v_{x,k}^m$  is the mean velocity of the two rear wheels. This is obtained from the Motor RPM using 5.

$$v_{x,k}^m = \frac{\text{Motor RPM} * \text{Tire Circumference}}{60 * \text{Gear Ratio}} \quad (5)$$

The longitudinal velocity is an element in both the system state and the measurement vector in equation (4), the EKF serves as a filter to for the measured wheel angular speed. This helps reduce the effect of the measurement noise on the tire side-slip angle.

#### B. UKF1: Force Estimation

The two Unscented Kalman Filters are implemented sequentially to determine the tire force as well as the Tire-Road Friction Coefficient Estimation (TRFC) as can

be seen in the flowchart in 2. The state and measurement vectors for UKF1 shown in equation 6 are a combination of both sensor inputs as well as the lateral and longitudinal velocity given by the EKF and is given as:

$$\begin{aligned}x_k^U &= [v_{x,k}, z_{k,z}, v_{y,k}, F_{xf,k}, F_{yf,k}, F_{yr,k}] \\ z_k^U &= [\hat{v}_{x,k}, \hat{z}_{k,z}, \hat{v}_{y,k}, a_{x,k}, a_{y,k}]\end{aligned}\quad (6)$$

The tire forces are the unknown states that need to be estimated from the UKF1 and are initialised to zero as a starting estimate. Governing equations of motion of the vehicle, along with the together with equation 6 are used to formulate the discrete-time state-space system model by integrating the process and measurement noises which we consider as negligible, as

$$\begin{aligned}x_k^U &= f^U(x_{k-1}^U, u_k^U) + w_k^U, \text{ where } w_k^U \sim N(0, Q^U) \\ z_k^U &= h^U(x_k^U) + v_k^U, \text{ where } v_k^U \sim N(0, R^U)\end{aligned}\quad (7)$$

The process noise covariance  $Q^u$  and the measurement noise covariance  $R^u$  is given as

$$\begin{aligned}Q^U &= \text{diag}([10, 107, 103, 400, 850, 675] * 100) \\ R^U &= \text{diag}([20, 94, 20, 86, 65])\end{aligned}\quad (8)$$

The dynamic function for the first UKF is given in equation 9 below

$$\begin{aligned}f^U &= [f_1^U, f_2^U, f_3^U, f_4^U, f_5^U, f_6^U] \\ f_1^U &= v_{x,k-1} + T_s *_{z,k-1} v_{y,k-1} \\ &\quad + \frac{T_s}{m} [F_{xf,k-1} \cos \delta_k - F_{yf,k-1} \sin \delta_k] \\ f_2^U &= z_{k,z} + T_S \frac{l_f}{I_z} [F_{xf,k-1} \sin \delta_k \\ &\quad + F_{yf,k-1} \cos \delta_k] - T_s \frac{l_r}{I_z} F_{yr,k-1} \\ f_3^U &= v_{y,k-1} - T_s *_{z,k-1} v_{x,k-1} \\ &\quad + \frac{T_s}{m} [F_{xf,k-1} \sin \delta_k + F_{yf,k-1} \cos \delta_k + F_{yr,k-1}] \\ f_4^U &= F_{xf,k-1}, f_5^U = F_{yf,k-1}, f_6^U = F_{yr,k-1}\end{aligned}\quad (9)$$

In our formulation, because of the low speeds involved, we assume that the motion resistance is only due to rolling resistance and that the aerodynamic drag forces are negligible. We find our sigma points using Cholesky Decomposition. The UKF parameters, together with the dimension of the state vector (6) determine the distribution of our sigma points and the corresponding weights.

The observation function for the same UKF is defined

in equation 10

$$h^U = \begin{bmatrix} h_1^U \\ h_2^U \\ h_3^U \\ h_4^U \\ h_5^U \end{bmatrix} = \begin{bmatrix} v_{x,k} \\ ohm_{z,k} \\ v_{y,k} \\ \frac{1}{m}[F_{xf,k}\cos\delta_k - F_{yf,k}\sin\delta_k] \\ \frac{1}{m}[F_{xf,k}\sin\delta_k - F_{yf,k}\cos\delta_k + F_{yr,k}] \end{bmatrix} \quad (10)$$

### C. UKF2: TRFC Estimation

By this stage, we have obtained the lateral tire forces  $\hat{F}_{yf}, \hat{F}_{yr}$  of the two axles, the side-slip angles of the front and rear-axles  $\alpha_f, \alpha_r$  as well as the normal forces for both the axles  $F_{zf}, F_{zr}$ . We also assume that the corner stiffness of the axles are constant (check appendix). The final UKF is used to measure the Tire-Road Friction Coefficients by considering the TRFC as a vehicle state within the 'tire-brush' model. The tire-brush model is described discrete-time nonlinear system as

$$\begin{aligned} \tau_k &= \tau_{k-1} + w_k^B, \text{ where } w_k^B \sim N(0, Q^B) \\ z_k^B &= h_B(\tau_k) + v_k^B, \text{ where } v_k^B \sim N(0, R^B) \end{aligned} \quad (11)$$

The process noise covariance  $Q^B$  and the measurement noise covariance  $R^B$  is given as

$$\begin{aligned} Q^B &= \text{diag}([10^{-4}, 10^{-4}]) \\ R^B &= \text{diag}([10^4, 10^4]) \end{aligned} \quad (12)$$

## IV. EXPERIMENTAL RESULTS

### A. Datasets:

To test out our filtering hierarchy, we collected a total of 5 datasets from a range of different floor materials. The datasets have been collected from the following environments:

- 1) **Dataset 1:** Compressed concrete outside of Levine Hall main entrance.
- 2) **Dataset 2:** Dirty tile environment from the second floor of Levine Hall.
- 3) **Datasets 3 through 5:** Varying environments including carpet, tile and concrete from three hallways. The distribution of these environments is shown in figure 3. Going clockwise from the top-left, we get concrete-tile, tile, concrete, and carpet.

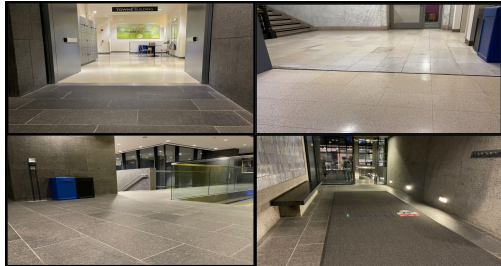


Figure 3: Floor environments for datasets 3 through 5.

The datasets are logged using a custom ROS node running in real-time on the  $F1/10^{th}$  car. The car was remotely operated using a joystick by a human operator to ensure desired trajectories are followed. The datasets are designed as the following runs:

- 1) **Dataset 1:** Three laps around the outdoors Levine track. First lap is slow, second lap is faster with slaloms, and the last is ran as fast as possible with slaloms.
- 2) **Dataset 2:** Three laps around the second-floor Levine Hall. First lap is slow, second is faster with slaloms, and the last is ran as fast as possible with slaloms.
- 3) **Dataset 3:** One slow run across the hallways of Towne, Moore, and Skirkish buildings and back, with slaloms on the way back.
- 4) **Datset 4:** One fast lap with slaloms across the hallways of Towne, Moore, and Skirkish buildings.
- 5) **Dataset 5:** Mixed speed lap with slaloms across the hallways of Towne, Moore, and Skirkish buildings.

Datasets 1 and 2 were used for tuning the EKF velocity estimator and the UKF force estimator by comparing estimates with particle filter estimates as ground truths. Datasets 3 and 4 include LIDAR scan data if needed for custom SLAM implementation. Dataset 5 includes raw motor RPM data read from the motor speed controller (VESC). This motor speed was added upon realization of the discrepancy between actual vehicle speed (PF ground truth) and our filter's estimate from the Ackermann ROS messages being used as input. This descrepancy is caused by the mismatch between the control input sent by ROS and the actual control command used by the VESC for the following reasons:

- 1) **Transmission Slip:** Due to imperfections in the vehicle, motor torque is not completely translated to wheel speeds due to clutch slipping.
- 2) **Delay:** Due to lag introduced by ROS, bluetooth and general system latency, the message sent over the ROS messaging bus is not instantaneously translated to motor speeds.
- 3) **VESC Saturation:** Arguably the most important factor and the one that made this issue notable. The VESC driver has inbuilt maximum speed limits that are set before each dataset run to ensure consistent max speeds. For dataset 3, this was set at a maximum of 2 meters per second, while the ROS messages still sent velocity messages of 5 meters per second. This discrepancy resulted in estimates of speed that are off by 3 meters per second which messes up the final estimates of the friction coefficients.

To counteract this discrepancy, we opted towards using the particle filter's estimate as the observed rear track

mean speed instead of the Ackermann command message. The resulting plots of our estimates are visualized next.

### B. Results and Analysis:

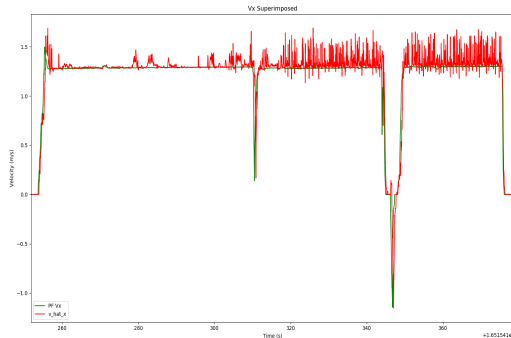


Figure 4: Longitudinal (x-axis) velocity measured by the particle filter and that estimated by our filtering hierarchy.

that the tire longitudinal force is not translated in whole to vehicle motion due to rolling resistance and fricative losses.

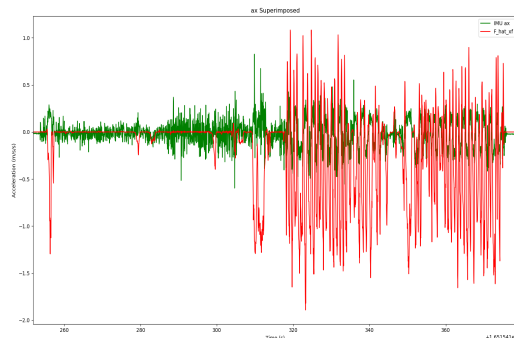


Figure 6: Longitudinal (x-axis) acceleration measured by IMU superimposed with force estimate converted to acceleration ( $F/m$ )

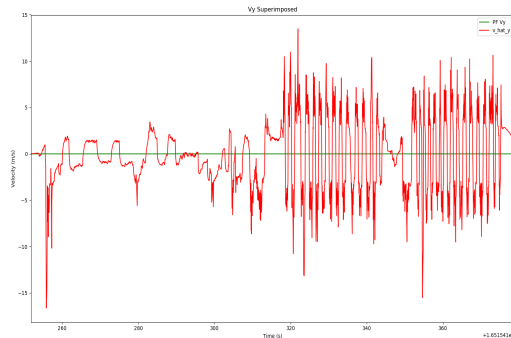


Figure 5: Lateral (y-axis) velocity measured by the particle filter and that estimated by our filtering hierarchy.

As can be seen in figure 4, our filter is capable of tracking the particle filter's estimated velocity throughout the dataset. Additionally, we note that the particle filter is incapable of measuring lateral velocities in minute precision as our filter can. With that said, we acknowledge that our lateral velocity estimates suffer from a scale factor error whose source we are unsure of. To negate this scale difference, the forces in the next stage of our filter are scaled by a factor of 100 to accommodate for this scale error. This factor of 100 was calculated by appropriating the differences between our estimate longitudinal tire force  $\hat{F}_x$  and the total longitudinal force experienced by our vehicle  $f_x$  as measured by our IMU's longitudinal acceleration times the vehicle's mass  $f_x = ma_x$ . This value was not tuned to be a 1-1 mapping as we know

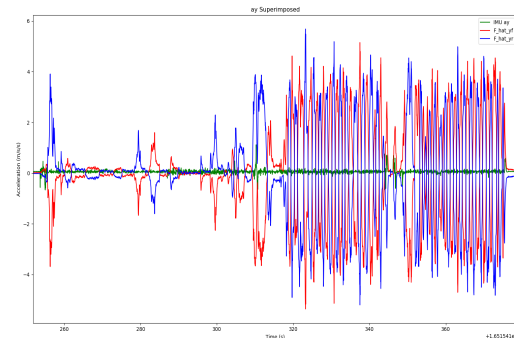


Figure 7: Lateral (y-axis) acceleration measured by IMU superimposed with force estimate converted to acceleration ( $F/m$ )

Initially, we had expected our tire-forces to better match the accelerations measured by the IMU. However, considering that these forces plotted are the forces experienced by individual wheels. The sum of these forces results in longitudinal and lateral motion as well as yaw. This can be clearly seen from the estimates of the cornering forces of our tires which show opposing forces whenever the car experiences yaw changes from slaloms.

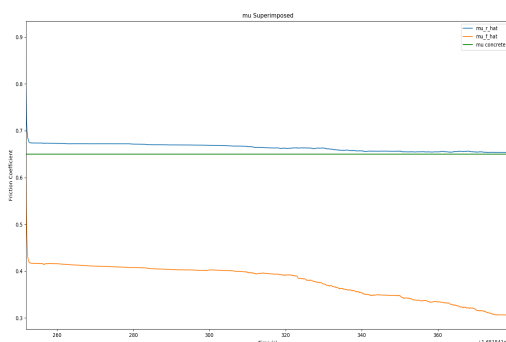


Figure 8: Friction Estimates superimposed with the friction coefficient of rubber on concrete

While we do not have a reference ground truth with which to compare these estimates with, we could compare these esimaates with the friction coefficient of rubber on dry concrete as visualized in figure 8. Even then, we had expected our estimates to vary much more abruptly with time as our car drives between the different environments. With that said, we can obtain a meaningful visualization as seen in 9. This visualization is obtained by taking the time period pertaining to the forward run in the map and extracting the friction estimates from that window. These estimates are then normalized to a range of 0 to 1 to exaggerate the differences in friction and the resulting changes can be clearly seen on the map as correlating with changes in surface material as expected, with the highest friciton occuring at the end at the carpet material, and the lowest at the start on tile.



Figure 9: Scaled Friction Estimates superimposed with occupancy grid.

## V. DISCUSSION

As can be seen, our estimates are far from perfect and our friction estimates do not model the changes in surface conditions. Even though our first two filters are capable

of producing acceptable estimates, this is not enough to produce the desired results. As such, we acknowledge the need for greater fidelity in our model, as well as the use of additional sensors, most notably, wheel speed sensors for more accurate measurements of wheel speeds. Had we had more time and funding for this project, we would have attempted to model our system as a two-track model and added wheel-speed sensors for greater accuracy in our estimates. Finally, we note that it is not possible to use any of these friction estimates as features to any SLAM algorithm in this current state as these features are redundant in the current form as the environment is uniform according to our current estimates. As such, it is necessary that more accurate models of the vehicle are used before friction can be used as a SLAM observation.

## VI. APPENDIX

$a_x$	Vehicle Longitudinal Acceleration
$a_y$	Vehicle Lateral Acceleration
$C_r$	Coefficient of rolling resistance(0.02)
$C_{yf}$	Front axle cornering stiffness(150)
$C_{yr}$	Rear axle cornering stiffness(150)
$F_{xf}$	Front-Axle Longitudinal Force
$\hat{F}_{xf}$	Estimated Front-Axle Longitudinal Force
$F_{xr}$	Rear-Axle Longitudinal Force
$F_{yf}$	Front-Axle Lateral Force
$\hat{F}_{yf}$	Estimated Front-Axle Lateral Force
$F_{yr}$	Rear-Axle Lateral Force
$\hat{F}_{yr}$	Estimated Rear-Axle Lateral Force
$F_{zf}$	Front-axle normal force
$F_{zr}$	Rear-axle normal force
$g$	Acceleration due to gravity ( $9.81 \text{ m/s}^2$ )
$h_c$	Height of the center of gravity of the car CG(0.075m)
$I_z$	Vehicle yaw moment of inertia ( $0.0687 \text{ kg.m}^2$ )
$l$	Vehicle wheel base
$l_f$	Distance from CG to front axle
$l_r$	Distance from CG to rear axle
$m$	total vehicle mass (3.3325 kg)
$T_s$	Sampling interval
$v_x$	Vehicle longitudinal velocity
$\hat{v}_x^k$	Filtered wheel speed
$v_{x,k}^m$	Mean velocity of the rear wheels
$v_y$	Vehicle lateral velocity
$\hat{v}_y$	Estimated vehicle lateral velocity
$\alpha_f$	Front tire side-slip/slip angle
$\alpha_r$	Rear tire side-slip/slip angle
$\delta$	Tire steer angle
$\mu_f$	Tire-road friction coefficient at front tires
$\mu_r$	Tire-road friction coefficient at rear tires
$\omega_{rl}$	Angular speed of rear-left wheel
$\omega_{rr}$	Angular speed of rear-right wheel
$\Omega_z$	Vehicle yaw rate

## REFERENCES

- [1] Admin. Slash 4x4 platinum: 1/10 scale 4wd electric short course truck with low cg chassis, Apr 2013.
- [2] Yuanyan Chen and Jim Zhu. Car-like ground vehicle trajectory tracking by using trajectory linearization control. page V002T21A014, 10 2017.
- [3] Jacob Svendensius. *Tire Modeling and Friction Estimation*. PhD thesis, Department of Automatic Control, 2007. Defence details Date: 2007-04-20 Time: 10:15 Place: Room M:B, M-building, Ole Römers väg 1, Lund Institute of Technology. External reviewer(s) Name: Limebeer, David Title: Professor Affiliation: Electrical and Electronic Engineering, Imperial Collage, UK.
- [4] Wenfei Li, Huiyun Li, Kun Xu, Zhejun Huang, Ke Li, and Haiping Du. Estimation of vehicle dynamic parameters based on the two-stage estimation method. *Sensors*, 21(11), 2021.
- [5] Song P. Hu D. Zong, Cf. Estimation of vehicle states and tire-road friction using parallel extended kalman filtering. *J. Zhejiang Univ. Sci. A* 12, 446–452 (2011), <https://doi.org/10.1631/jzus.A1100056>.
- [6] Hongyan Guo, Dongpu Cao, Hong Chen, Chen Lv, Huaji Wang, and Siqi Yang. Vehicle dynamic state estimation: state of the art schemes and perspectives. *IEEE/CAA Journal of Automatica Sinica*, 5(2):418–431, 2018.
- [7] Juqi Hu, Subhash Rakheja, and Youmin Zhang. Real-time estimation of tire-road friction coefficient based on lateral vehicle dynamics. *Proceedings of the Institution of Mechanical Engineers, Part D: Journal of Automobile Engineering*, 234:095440702092923, 06 2020.